Title
Abundances and Spectra for Cosmic-Ray Nuclei from Li to Fe For 2 to 150 GeV/n

Authors
Orth, Chalres D.
Ruffington, Andrew
Smoot, George F.
et al.

Publication Date
1978-03-27

Submitted to Astrophysical Journal

LBL-7553 c.2
Preprint

ABUNDANCES AND SPECTRA FOR COSMIC-RAY NUCLEI FROM Li TO Fe FOR 2 TO 150 GeV/n

Charles D. Orth, Andrew Buffington,
George F. Smoot, and Terry S. Mast

March 27, 1978

Prepared for the U. S. Department of Energy
under Contract W-7405-ENG-48
and the National Aeronautics and Space
Administration under grant NGR-05-003-553

ABUNDANCES AND SPECTRA FOR COSMIC-RAY NUCLEI FROM Li TO Fe FOR 2 TO 150 GeV/n

Charles D. Orth, Andrew Buffington, George F. Smoot, and Terry S. Mast

Space Sciences Laboratory and Lawrence Berkeley Laboratory
University of California, Berkeley

ABSTRACT

We report measurements of the absolute and relative abundances, differential energy spectra, and spectral indices for cosmic-ray nuclei from Li to Fe for 2 to 150 GeV/nucleon. These measurements were made using a balloon-borne superconducting magnetic spectrometer with scintillators and optical spark chambers. The abundances of Li, Be, and B for rigidities below 10 GV/c are consistent with an energy-independent mean interstellar pathlength of $4\frac{1}{2} \pm \frac{1}{2}$ g cm^{-2} for all propagation models. The abundances of all elements above 10 GV/c are consistent with an interstellar pathlength decreasing with rigidity as R^{-n} with an index $n = 0.6^{+0.4}_{-0.3}$. All differential source spectra can be fitted by power laws in total energy per nucleon with the same spectral index, which is between 2.5 and 2.6 depending on n. If n is near 0.5 (as for simple diffusion), the source index is 2.54 ± 0.03. Relative abundances at the sources are thus energy-independent, and have ratios to solar abundances as a function of first ionization potential which indicate a source temperature between 10^4 and 5×10^4 °K depending on the equilibrium nature of the injection environment.

Subject headings: Cosmic Rays -- composition and energy spectra; origin and propagation

Suggested Running Title: Cosmic-Ray Abundances and Spectra

I. INTRODUCTION

Measurements of the composition and energy spectra of primary cosmic-ray nuclei provide information about the mechanisms for cosmic-ray origin, acceleration, propagation, and galactic containment. Perhaps the most important recent observations above a few GeV/nucleon are the decreasing secondary/primary ratios. In particular, the L/M ratio (Li+Be+B+N)/(C+O) decreases by approximately a factor of two over the energy range from 5 to 50 GeV/nucleon (see references on figure 6 below). These observations have led to the development of new propagation models which explain the L/M decrease by having higher-energy nuclei traverse less material and thus generate fewer secondaries. Current interest is focused on just how and why the pathlength decreases at higher energies.

This paper describes new measurements of the primary cosmic-ray composition and energy spectra, and discusses the implications for various models of cosmic-ray propagation. The data were acquired during a September 1972 balloon experiment using a superconducting magnetic spectrometer. Preliminary results were presented by Smith, Buffington, Orth, and Smoot (1973a), and by Orth, Buffington, and Smoot (1975). Although similar in concept to our earlier experiment (Smith, Buffington, Smoot, Alvarez, and Wahlig 1973b), there were several important differences. The present experiment utilized a completely different gondola (Section II), and different charge-analysis techniques (Section III). Both of these changes were designed to reduce the possible systematic errors. In addition, we acquired twice as much data for charges $Z>8$ and comparable data for $Z\lesssim 8$.

Section IV presents our results for the absolute and relative integral abundances, the differential energy spectra, and the spectral indices for cosmic-ray nuclei from Li to Fe for 2 to 150 GeV/nucleon. Results are given both at 6.7 g cm^{-2} equivalent vertical atmospheric depth, and at the top of the atmosphere.

Section V shows that propagation effects can explain essentially all of the elemental observations. The treatment expands previous efforts (refs. in Section V) by including a wider range of charges and more than one propagation model.* We find that the abundances of Li, Be, and B below 10 GV/c are consistent with an energy-independent mean interstellar pathlength of $4\frac{1}{2} \pm \frac{1}{2}$ g cm^{-2} for any of the viable models. The abundances of all elements above 10 GV/c are consistent with a pathlength decreasing with rigidity as R^{-n}. The value of n depends on the constraints imposed while fitting the source spectra, but is $n = 0.6^{+0.4}_{-0.3}$ for the simplest assumptions. These assumptions permit the source spectra for all charges to be power laws in total energy per nucleon with the same spectral index, which is between 2.5 and 2.6 depending on n. If n is near 0.5, as for simple one-dimensional diffusion (Owens 1976a,b), the differential source spectral index is 2.54 ± 0.03. Relative abundances at the sources are thus energy-independent, and have ratios to solar abundances as a function of first ionization potential which indicate a source temperature between 10^4 and 5×10^4 °K depending on the equilibrium nature of the injection environment.

---

* The present work is also an expansion of Orth, Buffington, Mast, and Smoot (1977), in which we showed that our Fe/(C+O) data are consistent with the propagation effects commonly assumed to explain the (Li+Be+B+N)/(C+O) ratio.

II. APPARATUS AND DATA ACQUISITION

Figure 1 shows a schematic diagram of the superconducting magnet and detectors. Specifications for the apparatus are given in Smoot, Buffington, Orth, and Smith (1973), with additional details in Buffington, Orth, and Smoot (1974).

Triggering was accomplished by a 4-fold coincidence among scintillators S1 to S4. Thresholds were set by radio command to choose charges $Z \geq 3$ or $Z \geq 5$ (some $Z \geq 2$ data were acquired but not analyzed). The magnet anticoincidence (veto) could also be commanded IN or OUT of the trigger coincidence. The sparks, fiducial lights, clock, and digitized scintillator pulse-area data were recorded on 35 mm film using two cameras with wide-angle lenses. The geometry factor for the apparatus was 0.112 ± 0.002 m^2sr.

The apparatus was launched from Palestine, Texas on the evening of 30 September 1972 and flew at a residual atmospheric depth of 5.5 ± 0.2 g cm^{-2} (35.5 km) and a mean geomagnetic cutoff of 4.5 ± 0.1 GV/c. Table 1 summarizes the data analyzed.

TABLE 1: MAGNET-ON DATA ANALYSIS

Charge Mode Veto IN/OUT of trigger	$Z \geq 3$ IN	$Z \geq 5$ OUT	Total
Pictures Taken	41,062	6,144	47,206
Elapsed time in seconds	28,922	8,076	36,998
Events scanned good	27,702	5,370	33,072
Events measured	26,653	5,343	31,996
Events momentum fitted	26,288	5,343	31,631
Final events accepted*	12,082	3,616	15,698
Good scan events totally skipped	3,885	260	4,145
Live time in seconds, adjusted for events skipped and dead time of 0.2152 ± 0.0005 second/event	16,392 ± 23	6,312 ± 4	22,704 ± 23

*Excludes 1796 events failing fiducial-volume cuts, 2416 events with rigidities below 3.3 GV/c, 2794 events skipped as part of the live-time adjustment, 1619 events lost due to inefficiencies after the momentum-fitting stage, and all background and interacting events (4333 events with too few or too many sparks, characteristic of interactions or multiple tracks; 1711 events with bad trajectory fits; 1256 events failing the charge analysis counter-agreement tests; and 8 events assigned Z = 2).

III. DATA ANALYSIS

The methods of data analysis used here were almost identical to those of our previous experiment (Smith et al. 1973b), up to the point of charge analysis. The only major difference was that events inadvertently skipped during the film-measuring process and data analysis procedures were not retrieved here.

Table 1 outlines the event flow through the analysis. The pictures were scanned and measured, and the spark positions were reconstructed from the film plane to real space. Events with too few or too many sparks, due to multiple incident particles or interactions somewhere in the apparatus, were excluded. A rigidity (momentum per unit charge) was determined for each reconstructed event by least-squares fitting an allowed trajectory through the spark coordinates. Events were excluded which had a poor fit. Events with trajectories intersecting the veto or passing too near to the edges of the scintillators were excluded to permit the use of a single geometry factor. Finally, events below geomagnetic cutoff were eliminated.

a. Charge Analysis

The digitized scintillator pulse data were corrected for incident angle, saturation, position, and gains as in Smith et al. (1973b) to yield the expected Z^2 response. The square root of each pulse was taken to obtain an analog charge.

At this point the analysis diverged from that of our previous experiment. The old charge algorithm was based on proximity of an analog charge to an integer charge; this significantly distorted the division of events among neighboring elements with widely differing abundances, primarily for events with $9 \lesssim Z \lesssim 14$. In addition, we previously included some fragmenting events, classifying them according to the observed fragment, under the assumption that the experiment was thereby effectively flown at a slightly increased atmospheric depth. Here we excluded all events interacting in or between S1 and S2, thus removing a systematic uncertainty arising from the unknown fraction of interactions between S1 and S2 which failed the spark-chamber scanning and analysis criteria. This approach increased the attenuation correction for events fragmenting within the apparatus, but minimized the effective atmospheric depth at which the experiment was flown. The corrections thereby relied more on total cross section data and less on the imprecise partial cross sections needed for atmospheric corrections.

Fragmenting and interacting events were eliminated with an agreement test among the analog charges in combinations of four, three, or two counters as described in Appendix C. No event was accepted unless the confidence level for the chi-square of the analog charges about their mean was above 0.05. A Monte Carlo program showed that 99.8% of events not interacting in the spectrometer should pass these counter-agreement criteria, plus a negligible 1% of the events interacting before reaching the middle of S2. Since 13% of the incident events did interact by the middle of S2, we expected 87% of all incident events to pass the agreement tests. In fact, 93% of the good-scan flight data passed. The difference (6%) is the interaction fraction which failed the scanning criteria, and is therefore an indication of the systematic error which was incurred in Smith et al. (1973b) due to their charge-analysis procedures.

Figure 2 shows the spectrum of average analog charges for the accepted events, uncorrected for the effects of interactions within the apparatus.

Bin edges were defined near each minimum between the charge peaks so the overlap from adjacent charges was equal. Different shapes of the tails on the charge spectra were considered for neighboring charges with greatly differing abundances. Elemental abundances were determined by counting the events within these charge bins. We combined the abundances for $15 \leq Z \leq 24$ and $Z \geq 25$ into groups labelled respectively as P-Cr and Fe, because of the limited numbers of events and a charge resolution not as good as at lower Z. The results are described in Section IV.

b. Spectral Index Fitting

The sample of events selected for spectral-index fitting excluded the events with specific curvatures (inverse rigidities) $K > +0.12\ (GV/c)^{-1}$, as in the previous experiment, to make the fits insensitive to uncertainties in geomagnetic cutoff and solar modulation. We also excluded all events with negative specific curvatures because our antimatter-search analysis (Smoot, Buffington, and Orth 1975) showed some of these events had grossly mismeasured sparks and hence unreliable values of K.

Spectral fits were performed for each charge group separately. To reduce the contamination from neighboring charges, events were selected from narrowed versions of the charge bins defined for the abundance determinations. The narrowed bins had edges moved closer to the integers by amounts varying from zero charge units at Li to 0.2 charge units at Fe. The resulting fits were insensitive to the exact placement of the bin edges, and each fit was made with 80 to 100% of the data for that charge. Residual contamination from neighboring charges was less than 2%.

The fitting process began by estimating the error in specific curvature K for each event. Film-measurement accuracy was the predominant source of error (about 1/4 mm in real space per spark chamber). We excluded the 15% of the events near the edges of the geometry defined by SC2 coordinates larger than 25 cm transverse to the magnet axis, where the field integral was low (error in K large) and the camera-lens corrections were least accurate. The distribution of errors in K for the remaining sample had a mean of $(60\ \mathrm{GV/c})^{-1}$.

The K spectrum for each charge group was fit using a maximum likelihood method (Eberhard and Koellner 1972, 1973: fit type 13). The function fit was a normalized convolution of a power law in total energy per nucleon $dN/dE \sim E^{-\gamma}$ and a Gaussian resolution function in K. Here γ denotes the spectral index to be determined. Results of these fits are given in Section IV. To see if solar modulation were important, an additional fit was made which included a modulation factor $\exp(-\alpha K/\beta)$ for parameter α and speed βc. The fitted value of α was negligibly small.

c. Corrections for Interactions in the Apparatus and the Residual Atmosphere

The abundances determined in the charge analysis were corrected for interactions in the 1.9 g cm^{-2} of scintillator and 0.8 g cm^{-2} of Al + foam comprising the spectrometer (along a typical trajectory) from the top of S1 to the middle of S2 (cf. Table 2). Corrections were made using exponentials and the mean free paths from equation (A1) of Appendix A.

The abundances were also corrected for fragmentations in the 0.8 g cm^{-2} of fiberglass and foam comprising the gondola shell, and in the 5.5 g cm^{-2} of residual atmosphere (5.9 g cm^{-2} after correction for the median cosine for incident particles). The procedure used to make the corrections is described in Appendix B. The corrections were partly multiplicative and partly additive, but were expressed as overall factors (cf. Table 2).

d. Efficiency

Inefficiency in the trigger system electronics was negligible for $Z \geqslant 5$, since the veto was overridden for these charges. A small and slightly rigidity-dependent inefficiency, averaging only 0.5% at Li and 0.9% at Be, was removed from the veto-IN data below boron to allow for events whose delta rays operated the veto. The abundances of Li and Be were also increased to offset their smaller exposure factor (Table 1).

The scanning efficiency was determined to be $98.7 \pm 0.3\%$ by multiple scanning much of the film. The efficiency of the film-measuring process was essentially 100%, excluding the data blocks inadvertently skipped. Multiple sparks and too few sparks caused approximately 10^4 and 6×10^3 events respectively to fail the reconstruction process. Re-examination and measurement of these events recovered respectively 81% and 34%. The rescan showed the unrecoverable events to be interactions, plus a few good events improperly treated in the recovery operation. The final efficiency of the reconstruction process for all good events was $95.6 \pm 0.2\%$. The total efficiency for good events passing all scanning, measuring, and reconstruction criteria was $94.2 \pm 0.3\%$.

The efficiency of the charge analysis procedure was 99.8%. An efficiency of 96.6% was incurred in the final analysis stage by choosing not to remeasure 546 events with specific curvatures between -0.3 and -0.02 $(GV/c)^{-1}$. In summary, excluding the events totally ignored in the early analysis stages, the efficiency of the data analysis relating to the integral abundances was $90.8 \pm 0.4\%$.

For results pertaining to the spectral-index fits, we excluded the 339 events with specific curvatures K between -0.02 and 0.00 $(GV/c)^{-1}$

and the 2,292 events with large uncertainties in K (due to SC2 coordinate transverse to the magnet axis larger than 25 cm). The efficiency of the data analysis was thereby lowered to 75.6 ± 0.4%. We chose to use these same restrictions in obtaining the differential energy spectra for two reasons. First, the differential spectra were extrapolated back to the cosmic-ray sources and fit to power laws, and we wanted to be able to compare the spectral indices obtained there with those obtained at the gondola in the absence of any rigidity dependence in the mean interstellar pathlength. Second, the reported differential fluxes are a function of the spectral indices (especially at high energies) through the corrections for spillover from one rigidity bin to another due to measurement errors, and through the calculation of the effective size of each bin. Systematic errors are therefore minimized for the differential spectra when they are minimized for the spectral-index determinations.

e. Systematic Errors

Because the abundances reported by different groups have often disagreed by more than statistical errors would allow, a discussion of the possible systematic errors in each phase of an experiment is essential. First we note that our apparatus has been used in other measurements, and is well understood. The results of the search for antimatter in this experiment were reported by Smoot, Buffington, and Orth (1975). The same instrument was used to collect electron and positron data (Buffington, Orth, and Smoot 1975).

Backgrounds were minimized in this experiment through the use of optical spark chambers, which provided visualization of each event. The acceptance of only allowed trajectories through the magnetic field reduced the backgrounds to a negligible level.

Systematic errors in the assignment of charge were greatly reduced by the use of four independent charge measurements for the majority of the events. The charge algorithm was checked with a Monte Carlo program. Statistically similar abundances were obtained when only S1 was used to assign charges. In addition, re-analysis of the data of our previous experiment (Smith et al. 1973b) using the new techniques gave results in satisfactory agreement with those presented here (Section IV). Based on the small overlap uncertainty between adjacent peaks in the charge spectrum, we estimate the systematic error in the relative abundances from the possible misassignment of charge to be about 0.2 of the statistical uncertainty except for $Z = 9$, 11, and 13, where it is still less than half of the statistical uncertainty.

Two other sources of systematic error are the corrections for interactions within the spectrometer and the corrections for fragmentations in the atmosphere. Both rely on our choice of total and partial fragmentation cross sections, which are uncertain to perhaps 10% and 15% respectively. Because these uncertainties are expected to be highly correlated from one element to another, their effect cannot be included simply by quadraturing the uncertainties with statistical errors. For this reason, we calculated the effect of a coherent 10% reduction in all interaction cross sections; the results are given in Table 3 (last column). The element most affected is Be, whose absolute flux changed 9%.

Additional systematic uncertainty for the apparatus corrections may have arisen from the choice of the middle of S2 as the depth within the spectrometer where interactions were effectively rejected. Monte Carlo studies indicated that this choice would result in corrected abundances accurate to better than 2% for all Z.

Interactions in or above the shell were assumed to yield nuclei unaccompanied by secondaries visible in the spectrometer, even though this is not always true. Little systematic error was incurred with this procedure, however, because the correction for the shell was small compared to the atmospheric correction.

The specific curvature for each event was determined by measuring the trajectory on the film. Inflight calibration data taken after the magnet was turned off provided a check on this simple geometric determination, and established the resolution as $(60\ \mathrm{GV/c})^{-1}$. The absolute scale of specific curvature was found to be 2% low in a subsequent experiment with the same apparatus (Buffington, Orth, and Mast 1978). We don't know whether this scale normalization applies to the present experiment, but if so, the only effect would be to lower our differential fluxes by 3%.

During the spectral-index fitting, spillover of events from one rigidity bin to another due to normal measurement errors was automatically included, so no special correction was necessary. Elimination of the events with negative specific curvatures reduced the systematic error due to grossly mismeasured sparks. An estimate of the effect of residual contamination on the spectral indices is $\Delta\gamma < 0.05$ for all Z except Na and P-Cr, and $\Delta\gamma < 0.12$ for them (cf. Table 5). The maximum systematic error in the spectral indices due to miscalibration of the origin of specific curvature is about 0.02.

In summary, we estimate the systematic error is 10 to 15% for both the differential and the relative fluxes reported in Section IV, and no more than about 0.05 for all spectral indices except those for Na and P-Cr.

IV. EXPERIMENTAL RESULTS

a) Absolute Fluxes

We observed 4533 carbon events with an exposure factor of 2550 m^2 sr sec and an efficiency of 91%. The observed absolute integral flux of carbon was hence 2.0 ± 0.1 $(m^2 \text{ sr sec})^{-1}$ at the gondola, above an average geomagnetic cutoff of 4.5 GV/c. When corrected for interactions in the apparatus (Table 2), this becomes 2.2 $(m^2 \text{ sr sec})^{-1}$ at an equivalent vertical atmospheric depth of 6.7 g cm^{-2}. At the top of the atmosphere, the flux is 2.6 ± 0.1 $(m^2 \text{ sr sec})^{-1}$. This is in agreement with the second-flight value measured by Smith et al. (1973b), and with the 2.63 ± 0.08 above 4.35 GV/c reported by Von Rosenvinge, Webber, and Ormes (1969). Our C+O absolute flux at the top of the atmosphere is 5.1 ± 0.2 $(m^2 \text{ sr sec})^{-1}$ above 4.5 GV/c, somewhat larger than the 3.45 ± 0.70 above 4.5 GV/c quoted by Balasubrahmanyan and Ormes (1973).

b) Relative Integral Abundances

Integral abundances relative to carbon are listed in Table 2, along with the analysis steps used to obtain them. The abundances above 4.5 GV/c at 6.7 g cm^{-2} were converted to abundances above 2.4 GeV/nucleon prior to atmospheric correction primarily because we feel acceleration mechanisms at the cosmic-ray sources are more likely to involve energy changes than rigidity changes (see e.g. Scott and Chevalier 1975). We have therefore chosen to express all results in units of total energy per nucleon. The reconversion to rigidity in column eight of Table 2 was done merely to facilitate a direct comparison with both the results of Smith et al. (1973b), and our reanalysis of that experiment using the more recent cross-section data and our new charge-selection procedures. The reanalysis improved the accuracy in the Z = 9 to 14 range, where improvement was expected, but

TABLE 2: <u>Abundances Relative to Carbon*</u>

Z Group	Observed # Events	Correction factors for interactions in apparatus	Relative Abundances at 6.7 g cm^{-2} depth: Measured >4.5 GV/c	Relative Abundances at 6.7 g cm^{-2} depth: Convert to >2.4 GeV/n	Atmospheric Correction Factors	Relative Abundances at Top of Atmosphere — Present Experiment: Calculated >2.4 GeV/n	Relative Abundances at Top of Atmosphere — Present Experiment: Convert to >4.5 GV/c ⧸	Relative Abundances at Top of Atmosphere — Smith et al. (1973b) Flight #2 >4.55 GV/c	Relative Abundances at Top of Atmosphere — Re-analysis of Smith et al. §
3	835	1.09	24.8±0.9	22.7±0.8	0.84	16.0±0.8	17.5±0.9	18.1±1.8	-------
4	428	1.10	12.7±0.6	12.6±0.6	0.74	7.9±0.6	8.0±0.6	4.2±0.8	6.0±0.4
5	1351	1.12	29.6±0.8	27.7±0.8	0.98	22.8±0.8	24.4±0.8	23.5±1.3	29.2±1.2
6	4533	1.13	100.0±1.5	100.0±1.5	1.19	100.0±1.6	100.0±1.6	100.0±2.4	100.0±2.3
7	1251	1.14	28.2±0.8	27.4±0.8	1.09	25.3±0.8	26.0±0.9	24.8±1.3	22.6±1.0
8	3882	1.15	87.4±1.4	87.7±1.4	1.28	94.6±1.6	94.3±1.5	94.0±2.3	104.6±2.5
9	135	1.16	3.1±0.3	3.0±0.3	0.79	2.0±0.3	2.0±0.3	2.1±0.7	2.2±0.3
10	597	1.17	13.6±0.6	13.3±0.5	1.22	13.6±0.6	13.9±0.6	18.9±1.3	16.6±1.0
11	169	1.18	3.9±0.3	3.6±0.3	0.99	3.0±0.3	3.2±0.3	0.8±0.5	2.4±0.3
12	728	1.19	16.9±0.6	16.8±0.6	1.30	18.3±0.7	18.5±0.7	23.6±1.4	21.7±1.1
13	181	1.20	4.2±0.3	4.1±0.3	1.16	4.0±0.4	4.1±0.4	1.8±0.5	5.9±0.6
14	563	1.20	13.2±0.6	13.3±0.6	1.33	14.9±0.7	14.8±0.7	19.6±1.3	18.2±1.1
15-24	614	1.25	14.9±0.6	14.4±0.6	1.28	15.5±0.7	16.1±0.7	18.1±1.4	17.6±1.0
≥25	431	1.30	11.1±0.5	10.4±0.5	1.57	13.7±0.7	14.6±0.7	12.0±1.1	15.0±1.1

* The uncertainties shown are statistical, and do not include carbon's uncertainty for Z ≠ 6 even though the abundances are normalized to carbon.

§ Z4-OUT mode only. The differences relative to the previous column for Z's outside the 9-14 interval are the result of different cross-section data and statistics.

⧸ To obtain absolute fluxes above 4.5 GV/c in events per m^2 sr sec above the atmosphere, divide the relative abundances by 38 (and add the 1.8% uncertainty in the geometry factor, live time, and efficiency in quadrature with the uncertainty indicated).

produced rather high abundances for B and O.

Our results are compared with previously published abundances in Table 3. Although there is qualitative agreement, some differences are larger than expected from the errors provided. The last column indicates the level of systematic uncertainty in our results.

c) Absolute Differential Spectra

The differential energy spectra at the top of the atmosphere are given in Table 4. These results include all corrections, including spillover from one bin to another. They were obtained by converting the fluxes measured at the gondola to fluxes in terms of total energy per nucleon, based on an assumed mean atomic weight for each Z (Appendix B). These fluxes were scaled to the mean energies for the carbon data using the fitted spectral indices (Table 5). Atmospheric corrections were then applied to each bin separately. The conversion to energy per nucleon and the scaling to mean energies increased the possibility of systematic error arising from misassessment of the correct mean atomic weights and spectral indices; however, these procedures are essential for proper extrapolation through the atmosphere and interstellar space for the high-energy bins, where the mean energies would otherwise differ significantly from one element to another. In addition, as explained above, we feel it is more physical to obtain source spectra in energy units.

Ratios of abundances at the top of the atmosphere can be obtained as a function of energy from Table 4 (see figures 3 to 6). Such ratios are, for the most part, consistent with the results of other groups. We see decreases with increasing energy for the (Li+Be+B+N)/(C+O) and (Ne+Mg+Si)/Fe ratios. The decrease in the (Li+Be+B+N)/(C+O) ratio is in good agreement with our previous measurement and the average decrease seen by others.

TABLE 3: Comparison of Relative Abundances at the Top of the Atmosphere

Charge Group	Webber et al. (1972)* >1.8 GeV/n	Badhwar and Osborn (1974) > 4 GV/c	Júliusson (1974) at 23 GeV/n	Arens and Ormes (1975)# >1.7 GeV/n	Benegas et al. (1975) 1.8-2.3 GeV/n	Julliot, Koch, and Petrou (1975) 1.3-7.GeV/n	Lund et al. (1975a,b)† >3 GeV/n	Present Experiment >2.4 GeV/n	Present Experiment Systematics§
3	14.6±0.7		4.8±10.4	25.5±3.0		20.7±1.7		16.0±0.8	+1.2
4	8.5±0.5		2.9±4.3	12.1±1.5		9.3±0.9	9.0±1.6	7.9±0.6	+0.9
5	26.8±1.0	43±3	13±6	29.8±2.6		28.6±2.0	25.1±3.2	22.8±0.8	+0.9
6	100.0±1.8	100±6	100±12	100.0±2.2		100.0±4.0	100.0±3.3	100.0±1.6	0.0
7	24.1±0.9	54±3	21±5	29.2±4.5		24.4±1.5	28.6±2.4	25.3±0.8	+0.5
8	87.7±1.8	91±5	104±10	88.8±1.9		93.0	102.6±1.8	94.6±1.6	-1.3
9	1.1±0.2	8±1	3.6±1.7			0.9±0.3	2.1±0.6	2.0±0.3	+0.2
10	15.6±0.7	9±1	16±3	15.5±1.5		16.2±0.8	16.8±0.9	13.6±0.6	0.0
11	2.5±0.3	7±1	0.0±1.0	4.3±0.7		1.0±0.4	3.2±0.6	3.0±0.3	+0.2
12	18.1±0.7	16±2	15±3	16.8±0.7	19.3±1.5	20.7±0.9	22.7±0.9	18.3±0.7	-0.3
13	2.3±0.3	8±1	3.1±1.7	2.5±0.5	4.3±0.6	2.4±0.5	4.2±0.5	4.0±0.4	+0.1
14	11.9±0.6	14±2	9±2	15.2±0.7	14.5±0.8	16.3±0.8	18.5±0.8	14.9±0.7	-0.3
15-24	11.4±0.6		7.5±3.9		13.8±0.6	~14±1	13.3±0.9	15.5±0.7	-0.1
≥25	10.7±0.5		13±3		=11 ±0.2	~13±1	13.1±0.5	13.7±0.7	-0.6

* Also see Von Rosenvinge, Webber, and Ormes (1969); and Lezniak and Webber (1975).

\# Also see Ormes et al. (1975), and Maehl et al. (1977).

† Also see Cassé et al. (1971).

§ Change in relative abundances due to a coherent 10% reduction in all interaction and spallation cross sections. The absolute change in the carbon abundance was -2.2%.

TABLE 4: Differential Fluxes at the Top of the Atmosphere

Particles / m^2 sr sec (GeV/n)

Mean Total Energy (GeV/n)† Charge Group	2.6	3.3	4.3	5.7	8.3	12.0	18.8	33.7	147.
3	1.1 ± 0.2^{-1}*	1.2 ± 0.1^{-1}	7.3 ± 1.0^{-2}	3.3 ± 0.4^{-2}	1.5 ± 0.2^{-2}	5.0 ± 1.1^{-3}	1.4 ± 0.5^{-3}	3.8 ± 1.5^{-4}	1.2 ± 0.7^{-5}
4	6.9 ± 1.5^{-2}	5.7 ± 1.0^{-2}	3.1 ± 0.7^{-2}	2.0 ± 0.4^{-2}	5.5 ± 1.8^{-3}	1.6 ± 0.8^{-3}	5.4 ± 3.4^{-4}	2.6 ± 8.4^{-5}	1.5 ± 3.1^{-6}
5	2.0 ± 0.2^{-1}	1.9 ± 0.1^{-1}	9.3 ± 0.9^{-2}	4.6 ± 0.4^{-2}	1.9 ± 0.2^{-2}	5.5 ± 1.0^{-3}	1.4 ± 0.4^{-3}	3.7 ± 1.3^{-4}	8.9 ± 4.8^{-6}
6	8.5 ± 0.4^{-1}	7.6 ± 0.3^{-1}	4.2 ± 0.2^{-1}	19.8 ± 0.9^{-2}	8.1 ± 0.5^{-2}	3.2 ± 0.2^{-2}	1.0 ± 0.1^{-2}	2.5 ± 0.3^{-3}	5.4 ± 1.3^{-5}
7	2.2 ± 0.2^{-1}	1.9 ± 0.1^{-1}	1.0 ± 0.1^{-1}	5.0 ± 0.5^{-2}	2.0 ± 0.2^{-2}	7.4 ± 1.2^{-3}	2.0 ± 0.5^{-3}	7.0 ± 1.8^{-4}	8.2 ± 5.5^{-6}
8	7.5 ± 0.4^{-1}	7.3 ± 0.3^{-1}	3.9 ± 0.2^{-1}	19.9 ± 0.9^{-2}	7.9 ± 0.5^{-2}	3.0 ± 0.2^{-2}	1.2 ± 0.1^{-2}	3.0 ± 0.4^{-3}	1.1 ± 0.3^{-4}
9	3.5 ± 5.0^{-3}	7.9 ± 4.0^{-3}	6.8 ± 3.2^{-3}	5.6 ± 1.7^{-3}	4.8 ± 6.6^{-4}	1.1 ± 0.5^{-3}	4.9 ± 2.4^{-4}	2.3 ± 1.1^{-4}	$8.\ \pm49.^{-6}$
10	1.1 ± 0.1^{-1}	1.1 ± 0.1^{-1}	5.5 ± 0.7^{-2}	2.7 ± 0.3^{-2}	1.1 ± 0.2^{-2}	3.7 ± 0.9^{-3}	1.9 ± 0.4^{-3}	2.0 ± 1.0^{-4}	1.2 ± 0.8^{-5}
11	2.3 ± 0.8^{-2}	2.6 ± 0.6^{-2}	1.3 ± 0.4^{-2}	4.8 ± 1.6^{-3}	1.1 ± 0.8^{-3}	9.1 ± 4.5^{-4}	3.3 ± 1.9^{-4}	0# $\pm2.5^{-5}$	0# $\pm4.5^{-7}$
12	1.5 ± 0.2^{-1}	1.3 ± 0.1^{-1}	7.3 ± 0.8^{-2}	4.1 ± 0.4^{-2}	1.9 ± 0.2^{-2}	5.3 ± 1.0^{-3}	1.7 ± 0.4^{-3}	4.7 ± 1.5^{-4}	9.0 ± 4.8^{-6}
13	3.3 ± 0.9^{-2}	3.3 ± 0.6^{-2}	1.9 ± 0.5^{-2}	6.8 ± 1.9^{-3}	3.6 ± 1.1^{-3}	1.4 ± 0.6^{-3}	6.1 ± 2.6^{-4}	9.9 ± 7.5^{-5}	5.9 ± 5.7^{-6}
14	1.4 ± 0.2^{-1}	1.1 ± 0.1^{-1}	5.2 ± 0.7^{-2}	3.1 ± 0.4^{-2}	1.2 ± 0.2^{-2}	3.9 ± 0.9^{-3}	1.2 ± 0.4^{-3}	5.0 ± 1.6^{-4}	1.5 ± 0.9^{-5}
15-24	1.3 ± 0.2^{-1}	1.0 ± 0.1^{-1}	6.3 ± 0.8^{-2}	3.0 ± 0.4^{-2}	1.2 ± 0.2^{-2}	4.9 ± 1.0^{-3}	1.0 ± 0.4^{-3}	4.0 ± 1.5^{-4}	2.4 ± 3.3^{-6}
≥25	1.3 ± 0.2^{-1}	9.2 ± 1.0^{-2}	5.3 ± 0.7^{-2}	2.7 ± 0.4^{-2}	1.0 ± 0.2^{-2}	4.3 ± 1.0^{-3}	2.0 ± 0.5^{-3}	6.9 ± 2.0^{-4}	1.3 ± 1.3^{-5}

† Based on fitted spectral indices and the following lower bin edges in rigidity: 4.5, 5.5, 7.5, 9.5, 14., 20., 30., 50., and 100 GV/c.

* i.e. $(1.1\pm0.2) \times 10^{-1}$. Statistical errors shown exclude the 1.8% uncertainty in the geometry factor, live time, and efficiency, but include uncertainties in 1) the observed event count, 2) the effective sizes of the energy bins (which were based on the fitted power laws), and 3) the spillover corrections, which removed the effects of events spilling from one bin to another due to spark measurement errors. The effects of geomagnetic cutoff have not been removed from the first (and second) columns.

\# Zero events were observed in these bins.

TABLE 5: Spectral Indices for the Differential Energy Spectra

Z Group	This Experiment >8.3 GV/c Events	γ*	Smith et al. (1973b) >8.3 GV/c	Balasubrahmanyan and Ormes (1973) 3-80 GeV/n	Júliusson (1974) 2-100 GeV/n #	Lezniak and Webber (1975) 10-50 GeV/n	Caldwell (1977) >6.3 GeV/n #
3	325	2.56±.11(.05)	2.67±.13	2.28±.15	2.95±.12		
4	158	2.80±.18(.05)	2.66±.12	2.6 ±.2	3.09±.14		
5	472	2.66±.10(.05)	2.76±.08	2.76±.13	2.95±.07	3.01±.12	3.35±.10
6	1670	2.51±.05(.04)	2.54±.04	2.52±.06	2.65±.02	2.69±.03	2.76±.06
7	431	2.56±.09(.01)	2.72±.09	2.73±.11	2.74±.03	2.95±.12	3.07±.10
8	1529	2.39±.05(.01)	2.52±.05	2.57±.06	2.53±.02	2.70±.03	2.67±.04
9	48	2.07±.22(.03)			2.67±.10		3.01±.21
10	200	2.43±.14(.02)			2.57±.03		2.88±.08
11	49	3.24±.39(.11)			2.66±.10		3.14±.25
12	276	2.61±.13(.01)			2.56±.03		2.60±.06
13	60	2.47±.22(.04)	2.52±.07	2.44±.07	2.61±.08		2.52±.10
14	191	2.46±.14(.03)			2.50±.03		2.63±.11
15-24	194	2.70±.15(.12)		2.1 ±.2	2.6 ±.3		2.64±.07
≥25	157	2.26±.14(.05)		2.0 ±.1	2.3 ±.2		2.50±.08

* These indices pertain to power laws in total energy per nucleon. Uncertainties outside parentheses are the statistical uncertainties; uncertainties inside parentheses are the estimated upper limits for the systematic errors. A convenient expression for the statistical uncertainty in each index γ arising from a fit of γ only (no other parameters) is $\Delta\gamma = [-\partial^2(\ln L)/\partial\gamma^2]^{-1/2} = (\gamma-1)/\sqrt{N}$ for N events, whenever the likelihood function L is a product of Gaussians. The uncertainties we report are about 30% larger than this due to the errors in measuring rigidities.

\# Only statistical errors are shown; systematic error is ± 0.10.

Our decreasing (P-Cr)/Fe ratio is in agreement with the results of Webber, Lezniak, and Kish (1973a) and Webber, Lezniak, Kish, and Damle (1973b). We see only a slight increase in the O/C ratio, in contrast with Júliusson (1974), but in agreement with Smith et al. (1973b), Badhwar and Osborne (1974), and Lund, Rasmussen, Peters, and Westergaard (1975a). The moderate rise in the Fe/(C+O) ratio is in sharp disagreement with the steep rise reported by Ormes and Balasubrahmanyan (1973) and supported by Arens and Ormes (1975), but is in general agreement with others.

Table 5 shows that our fitted spectral indices are generally smaller than those of Júliusson (1974), which are in turn smaller than those of Caldwell (1977).

V. PROPAGATION MODEL PARAMETERS AND SOURCE ABUNDANCES

This section describes how we inferred the values of the parameters in various models by propagating the differential fluxes of Table 4 back to the sources and fitting the resultant spectra with power laws in total energy per nucleon. We sought to determine a rigidity dependence of the interstellar pathlength which yielded the simplest source spectra for elements considered primary, and zero source abundances for elements considered totally secondary.

Previous treatments of this kind have obtained power-law parameterizations of the decreasing interstellar pathlength at high energies by considering just a few elements within the framework of the "leaky-box" propagation model. Júliusson, Cesarsky, Meneguzzi, and Cassé (1975) calculated the energy dependence of the pathlength required to make Be+B equal to zero at the sources, and obtained a power-law index of 0.49 ± 0.05. Lezniak, Webber, Kish, and Simpson (1977) derived an index of 0.365 from their N/O and B/(C+O) ratios, and suggested that a Kolmogorov spectrum (index = 1/3) might be applicable. Caldwell (1977), using the source abundances of Shapiro, Silberberg, and Tsao (1975), found that his measured B/O ratio was best fit by a power-law index of 0.59 ± 0.09. Ormes and Freier (1978) fit their own and other data for (Li+Be+B)/(C+O) and obtained an index of 0.4 ± 0.1.

Our approach involves essentially all of the elements, weighted by their statistical errors. We consider the phenomenological "leaky-box" model with homogeneous sources, the slab model with an exponential distribution of pathlengths, and comment about the 2-component closed-galaxy model of Peters and Westergaard (1977). Other propagation models, although possibly less viable (Orth and Buffington 1976), include the 2-component models of Cowsik and Wilson (1973), Rengarajan, Stephens, and Verma (1973), and Meneguzzi (1973). All of the models are expected to give qualitatively similar results at the energies reported here.

For totally secondary elements, only Li, Be, and B were chosen because their production cross sections are better known than most other secondaries. Moreover, their parents (mostly carbon and oxygen) have fragmentation mean free paths comparable to the mean interstellar pathlength, so only a crude interaction model is sufficient to give first-order results; this is not true for the sub-iron secondaries. Nitrogen was not considered, even though it is often included in the L/M ratio, because it is probably not totally secondary.

Motivated by figure 6, we began by parameterizing the interstellar pathlength as $x = x_o$ g cm^{-2} for rigidities R under about 10 GV/c and $x = x_o(R/10)^{-n}$ for R above 10 GV/c. A rigidity representation was chosen because of the prejudice that the leakage mechanism causing this effect probably involves magnetic fields. The source fluxes S_i were derived from fluxes F_i of Table 4 using the leaky-box expression

$$S_i = F_i \left[1 + (x/\lambda_i)(1 - f_{ii})\right] - \sum_{j>i} \left[f_{ji} F_j (x/\lambda_j)\right]$$

where λ_i are the interaction mean free paths in 75% H + 25% He by mass (Appendix A), and f_{ji} are the fragmentation parameters (Appendix B).

For simplicity, one might expect all cosmic ray nuclei to originate at the same sources, and experience the same rigidity-dependent leakage history. This would require all Z to have the <u>same</u> n, and probably the <u>same</u> source spectral index γ. To check this hypothesis, we performed power-law fits to the S_i for i = C, N, O, Ne, Mg, Si, and Fe while varying n, x_o, and γ. An average spectral index Γ and a corresponding chi-square were calculated for each case by weighting the fitted spectral indices by the inverse square of their uncertainties. Because the values of n and Γ associated with the minimum chi-squares were not sensitive to the assumed x_o, this quantity was set to minimize the departure of $(S_{Li}+S_{Be}+S_B)/ S_C$ from zero. The results were then $n = 0.63^{+0.42}_{-0.35}$, $\Gamma = 2.56 \pm 0.03$, and $x_o = 4.6 \pm 0.3$ g cm^{-2}. If n were allowed to vary over the range indicated by its errors, Γ varied between 2.5 and 2.6. For n = 0.5, the best values were $\Gamma = 2.54 \pm 0.03$ and $x_o = 4.3 \pm 0.3$ g cm^{-2}. All results were insensitive to the choice of 10 GV/c in the parameterization of x; use of either the last 6 columns of Table 4 (i.e. R $\gtrsim$ 9.5 GV/c) or the last 7 columns (R $\gtrsim$ 7.5 GV/c) gave the same results.

Similar results were obtained for the slab model with an exponential distribution of pathlengths having x as the mean pathlength ($n = 0.7 \pm 0.4$, $\Gamma = 2.58 \pm 0.04$, $x_o = 4.6 \pm 0.3$ g cm^{-2}). The slab model considered at most two interactions, however, so the true x_o is expected to be slightly smaller than 4.6 g cm^{-2} (Appendix B). Leakage from a galactic arm, as in the Peters and Westergaard (1977) closed-galaxy model, should also yield similar results because their "old" galactic component is not important at these energies.

When n and γ were not required to be the same for all Z, we found fitted values of $n \lesssim 0.6$ depending on Z, and fitted source spectral indices varying from 2.3 to 2.7. The weighted average n for all Z from Li to Fe except the limited-statistics interval from Z = 9 to 13 was $n = 0.3 \pm 0.1$.

The above results rely on the assumption that x_o is best determined by minimizing the sum of Li, Be, and B at the sources. Different results were obtained by considering each element separately. For example, for the leaky-box model with n = 0.5, zero Li at the sources required $x_o = 5.2 \pm 0.5$ g cm^{-2}, while zero B required $x_o = 4.7 \pm 0.4$ g cm^{-2}. Zero Be, on the other hand, required $x_o = 2.6 \pm 0.5$ g cm^{-2}; that is, one-third of the Be predicted to be at the top of the atmosphere on the basis of $x_o = 4.3$ g cm^{-2} and the source abundances described below was not observed. Although the possibility of systematic error in the production cross sections is largest for Be (cf. Section III.e), the expected total error is too small to explain these anomalous results. We therefore support our analysis of a subsequent experiment (Buffington, Orth, and Mast 1978) which indicates that one-half of the high-energy Be^7 (i.e. one-third of all Be) has decayed to Li^7. Since the decay products remain within the (Li+Be+B) sum, use of this sum to obtain x is appropriate.

Source abundances were determined for the leaky-box model with x_o = 4.3 g cm^{-2} and n = 0.5 for all Z. This was done by scaling all abundances S_i using a power law with $\Gamma = 2.54$, and fitting to energy-independent values. The results are shown in Table 6, where they are compared with the results of others. Statistically similar abundances were obtained for the leaky-box solutions with different n and different γ, and also for the slab model with an exponential distribution of pathlengths.

The temperature of the sources can be inferred from the ratios of the source and solar-system abundances once the equilibrium nature of the injection environment is known. If the degree of atomic ionization is governed by electronic collisions impeded by radiative and dielectronic

TABLE 6: Source Abundances Relative to Carbon

Element	Webber et al. (1972)	Cassé, Goret and Cesarsky (1975)	Shapiro and Silberberg (1975)	This Experiment*	Solar System Cameron (1973)	Ratio This Expmt./ Solar System	First Ionization Potentials⸸
C	100	100.0	100	100.0±2.8	100.0	1.00±0.03	11.3
N	11.0±1.6	12.7	11±2	11.3±1.5	31.7	0.36±0.05	14.5
O	106	108.4	109±2	114.9±3.0	182.2	0.63±0.02	13.6
Ne	16.9	12.9±1.1	15±2	11.1±1.3	29.2	0.38±0.04	21.6
Na	1.3±0.4	1.1±0.7	0.8±0.4	0.0±0.5	0.51	0.0	5.1
Mg	23.3	22.2	23±2	21.5±1.6	9.0	2.4±0.2	7.6
Al	2.1±0.4	3.1±0.4	2±1	3.2±0.8	0.72	4.5±1.1	6.0
Si	17.3	22.2	20.5±3	17.3±1.5	8.5	2.0±0.2	8.2
P-Cr	< 9	(S=2.4±0.4) (Ca=2.2±0.2)	7 ± 1	10.1±1.6	6.1	1.6±0.3	~ 9.1
Fe	21	23.6	23±3	22.4±1.6	7.6	3.0±0.2	7.9

* The errors for $Z \neq 6$ do not include the error for carbon even though the abundances are relative to carbon. Our result for F was 0.0 ± 0.6 .

⸸ Weast (1972)

recombination in a low-density plasma, the approach of Cassé and Goret (1973) can be used. Their numerical analysis would presumably yield about the same result for our data as for theirs ($T \approx 10^4$ °K) since our source data do not differ significantly from the data they used. On the other hand, if thermal equilibrium were to apply, the Saha equation (Allen 1955) would require an exponential relationship between the ratios of source and solar-system abundances, and the first ionization potentials (figure 7). Our result would then be $T = (4.9 \pm 0.2) \times 10^4$ °K (ignoring the data for Ne, whose solar-system abundance is not well known: see e.g. Cassé, Goret, and Cesarsky 1975). This result is substantially higher than that obtained from the dilute-plasma model. In either case, however, the temperature corresponds to only a few eV, so the initial acceleration/injection processes may indeed proceed through singly ionized states.

VI. DISCUSSION

We have described an experiment covering a wide range in energy (2 to 150 GeV/n) with high efficiency, good background rejection, and low systematic error. The experimental results were interpreted to yield more information about the sources and propagation mechanisms of cosmic rays.

A simple model which is consistent with the data is that cosmic rays originate in a hot region ($T \gtrsim 10^4$°K) with all nuclei being accelerated to the same power-law spectrum with index Γ between 2.5 and 2.6. The injection into the accelerating phase may even proceed through singly ionized states, since the above temperature corresponds to an energy of a few eV, and the abundances are consistent with the Boltzmann factors based on first ionization potentials (figure 7). Cassé, Goret, Cesarsky (1975), however, have pointed out that other reasonable possibilities exist. If the accelerated spectra have different spectral indices, we found these may range from 2.3 to 2.7. The simplest assumption, however, is that all indices are the same. Our result is then $\Gamma = 2.54 \pm 0.03$ which is consistent with the $\Gamma \sim 2.5$ expected from second-order Fermi acceleration in supernova remnants (Scott and Chevalier 1975; Chevalier, Robertson, and Scott 1976). It is not yet clear, however, whether the high temperature we found is consistent with the supernova-remnant environment (Chevalier 1977).

After and/or during the acceleration phase, the cosmic rays propagate through the magnetic fields of the interstellar medium, traversing a column density dependent on particle rigidity. For particles below about 10 GV/c, we inferred the mean column density of 75%H + 25% He by mass to be $x_o = 4\frac{1}{2} \pm \frac{1}{2}$ g cm^{-2} by minimizing the source abundance of Li+Be+B. This result is consistent with an earlier result $4.3^{+1.8}_{-1.2}$ g cm^{-2} derived from positron data (Orth and Buffington 1976), but is about 1 g cm^{-2} less than most previous analyses (e.g. Meyer, Ramaty, and Webber 1974; Ormes and Freier 1978). Expressed in terms of an equivalent column density of hydrogen, our result is approximately $x_o = 4 \pm \frac{1}{2}$ g cm^{-2}.

For rigidities above 10 GV/c, the mean column density can be parameterized as $x = x_o(R/10)^{-n}$. If n and the source spectral indices are different for each charge, we found $n \lesssim 0.6$ with a weighted average of $n = 0.3 \pm 0.1$. More simply, if all Z have the same source spectral index Γ and the same n, then Γ is between 2.5 and 2.6, and $n = 0.6^{+0.4}_{-0.3}$. The value $n = 0.5$ is expected from simple diffusion (e.g. Owens 1976a,b). More complicated mechanisms exist, however, such as a Kolmogorov turbulence spectrum ($n = 1/3$: see e.g. Lezniak et al. 1977), compound diffusion (Lingenfelter, Ramaty, and Fisk 1971), or diffusion in a dynamical halo (Owens and Jokipii 1977).

The above results are of great significance, for they show that one statistically acceptable interpretation permits all Z to be accelerated to the same power-law spectrum, and then escape through interstellar space with a rigidity dependence governed by simple diffusion. We thus find no need to invoke separate source mechanisms for any nuclear species, in constrast with Ramaty, Balasubrahmanyan, and Ormes (1973); all cosmic rays arrive at Earth with spectral indices differing from one another and from the common source index merely due to the fragmentation and diffusion processes experienced in interstellar space. These results are consistent with those of Júliusson et al. (1975), Lezniak et al. (1977), Caldwell (1977), and Ormes and Freier (1978) discussed in Section V, but are now based on a wider range of charges.

All viable propagation models yield the above results, since they are all equivalent to a leaky box at these energies. This is not the case at higher energies, where the closed-galaxy model's "old" component becomes important and effectively truncates the decreasing pathlength. Higher energies is also where other 2-component models might become incompatible with the measured positron/proton ratio (Orth and Buffington 1976). We must wait for results at these higher energies to make any distinction.

This work was supported by grant NGR 05-003-553 of the National Aeronautics and Space Administration, and by the Lawrence Berkeley Laboratory of the Department of Energy. We acknowledge the assistance provided by the National Scientific Balloon Facility in Palestine, Texas, without whose help the balloon flight would have been impossible. We thank L.H. Smith and L.W. Alvarez for their interest and support.

APPENDIX A: FRAGMENTATION MEAN FREE PATHS

Fragmentation mean free paths were derived from

$$\lambda_{BT} = A_T / (6 \times 10^{-4} \sigma_{BT}) \quad \text{g cm}^{-2}, \tag{A1}$$

$$\sigma_{BT} = 200 \, (A_B^{1/4} + A_T^{1/4} - 1.7)^2 \quad \text{mb}, \tag{A2}$$

where A_B and A_T are respectively the beam and target atomic weights, and the constant in (A1) is Avogadro's number multiplied by 10^{-27}. Equation (A2) is a fit made by one of us (C.D.O.) to the C^{12}, O^{16}, Ar^{40}, and Fe^{56} data of Lindstrom, Greiner, Heckman, Cork, and Bieser (1975a,b), and Lindstrom (1977). This fit is accurate to $\lesssim$ 10% for $12 \leq A_B \leq 56$ and all $A_T \leq 238$. It applies for interactions which change A_B by one or more, and is not accurate for A_B near 1 if A_T is near 1. For air, we used $A_T = 14.7$; for interstellar space, which is 75% H and 25% He by mass (Abell 1969), we used $1/\lambda_{space} = 0.75/\lambda_H + 0.25/\lambda_{He}$.

APPENDIX B: FRAGMENTATION CORRECTIONS

The integral abundances and the differential fluxes in each energy bin were corrected for the expected mean change in composition due to spallation of the incoming cosmic rays in either interstellar material or the atmosphere. Fragmentation corrections for interstellar space were derived using the leaky-box model, or the slab model with results averaged over an exponential distribution of pathlengths. Corrections for the atmosphere were derived using a fixed slab model.

The appropriate propagation equation for the leaky-box model is described in Section V. For the slab models, we used the matrix equations $D = M * E$ and $E = M^{-1} * D$, where D was a column vector of data observed at one level (top of S1, or top of atmosphere) and E was the corresponding column vector of extrapolated data (top of atmosphere, or at cosmic-ray sources). Matrix M included the exponentials and their integrals describing the probabilities for each nuclear species to interact zero, one, or two times and produce a certain daughter species by depth x_o g cm^{-2}. That is,

$$M_{ij} = \exp(-x_o/\lambda_i)\, I_{ij} + \int_0^{x_o} (dx/\lambda_j)\, \exp(-x/\lambda_j)\, f_{ji}\, \exp[-(x_o-x)/\lambda_i] + \sum_k \int_0^{x_o} (dx/\lambda_j)\, \exp(-x/\lambda_j)\, f_{jk} \int_0^{x_o-x} (dy/\lambda_k)\, \exp(-y/\lambda_k)\, f_{ki}\, \exp[-(x_o-x-y)/\lambda_i] \quad \text{(B1)}$$

where I is the identity matrix, the λ were computed from (A1), and the f_{ji} are the fragmentation parameters in Table 7. The third term in (B1), for double interactions, accounted for at most 4% of the total correction for the atmosphere, and was largest for F and Be. On the other hand, this term was important for interstellar space, where it accounted for anywhere from 1% to 30% of the correction. Without this term, x_o would have been

TABLE 7: FRAGMENTATION PARAMETERS FOR NUCLEI IN INTERSTELLAR SPACE AND AIR, IN FORMAT (SPACE/AIR)*

Parents: Atomic Wt:	Li 6.5	Be 8.1	B 10.6	C 12.1	N 14.4	O 16.1	F 19.0	Ne 20.5	Na 23.0	Mg 24.3	Al 26.6	Si 28.2	P-Cr 41.6	Fe 56.0
Daughters														
Li	.16/.09	.13/.13	.16/.13	.10/.07	.08/.07	.07/.05	.07/.06	.07/.06	.07/.06	.07/.06	.06/.05	.06/.05	.07/.07	.09/.09
Be		.05/.08	.15/.09	.07/.05	.06/.04	.05/.04	.07/.05	.09/.08	.08/.07	.07/.07	.07/.07	.07/.07	.06/.06	.05/.05
B			.08/.06	.28/.11	.16/.10	.11/.05	.10/.06	.11/.07	.09/.06	.08/.05	.07/.05	.07/.05	.05/.04	.04/.03
C				0/.06	.29/.14	.17/.13	.12/.10	.10/.10	.09/.08	.07/.07	.05/.05	.04/.05	.03/.03	.02/.03
N					0/.05	.29/.13	.19/.12	.13/.06	.10/.05	.08/.04	.07/.04	.06/.03	.04/.02	.02/.02
O						0/.05	.28/.12	.21/.11	.17/.09	.15/.08	.12/.07	.10/.06	.06/.04	.03/.02
F							0/.05	.14/.08	.10/.07	.05/.06	.04/.04	.04/.04	.02/.03	.01/.02
Ne								0/.05	.23/.09	.20/.08	.16/.07	.13/.06	.08/.04	.03/.01
Na									0/.04	.14/.07	.10/.06	.05/.05	.03/.03	.01/.01
Mg										0/.05	.23/.09	.19/.09	.11/.06	.04/.02
Al											0/.04	.14/.05	.07/.05	.03/.03
Si												0/.04	.15/.09	.07/.04
P-Cr													.30/.14	.64/.31
Fe														.21/.09

* Each entry is the product of the probability to produce that daughter and the mean number of such daughters produced. All decays with lifetimes under 10^6 years have been allowed for the parameters in space; all decays with lifetimes under 10^{-4} second have been allowed for the parameters in air.

a factor of about 1.4 larger than the result obtained in Section V. This importance merely reflects the fact that interaction mean free paths in interstellar space are factors of three to six smaller than in the atmosphere.

The fragmentation parameters listed in Table 7 were compiled by determining the isotopic fragmentation cross sections for a hydrogen target, from the following sources: 1) from the $\Delta A_B \gtrsim 1$ data of Lindstrom et al. (1975a,b) and Lindstrom (1977); 2) from the semi-empirical formalism of Silberberg and Tsao (1973) for incident Ne, Mg, Si, and Fe; and 3) through interpolation from neighboring interactions of a similar character (e.g. neutron stripping). For interactions in interstellar space, all cross sections were modified to include the effects of the decays of isotopes with half lives under 10^6 years. Fragmentation parameters were obtained by summing the cross sections for each fragment and dividing by σ_{BT} of equation (A2), except the Silberberg and Tsao cross sections were scaled by their quoted total inelastic cross sections.

Modification of the fragmentation parameters to air as a target material was accomplished by multiplying by the ratio of target factors, $A_T^{1/4}$ / $(0.66 + 0.028\ A_i)$ for fragment atomic weight A_i (Lindstrom et al. 1975a), and then multiplying by the ratio of σ_{BT} from equation (A2): $[(A_j^{1/4} - 0.7) / (A_j^{1/4} + 14.7^{1/4} - 1.7)]^2$ for incident atomic weight A_j. No modification was performed to get the parameters for interstellar space, although the material is really 75% H + 25% He by mass (Abell 1969). The accuracy of all fragmentation parameters is perhaps 10 to 20% on the average.

APPENDIX C: CHARGE ANALYSIS DETAILS

Fragmenting and interacting events were eliminated from the charge analysis through a counter-agreement test sequence applied to every event. For the k^{th} event, the sequence began by testing all N = 4 counters (S1, S2, S3, and S4) for agreement. This was done by deriving a confidence level from the chi-square χ_k^2 of the N analog charges P_{ik} about their mean μ_k. The chi-square included the effects of correlations among the P_{ik} through use of an error matrix E, a correlation matrix $C_{ij} = E_{ij}/(E_{ii}E_{jj})^{1/2}$, and $S = C^{-1}$,

$$\chi_k^2 = [\sum_{i,j=1}^{N} (P_{ik}-\mu_k)\ S_{ij}\ (P_{jk}-\mu_k)] \ / \ (\delta Z)^2 \qquad (C1)$$

where δZ was the experimental charge resolution given below. Off-diagonal entries for C_{ij} were typically 5% except for the S3-S4 combination, which was 20%. The error matrix was calculated for all M events from

$$E_{ij} = [\sum_{k=1}^{M} (P_{ik}P_{jk}) - M\,\mu_i\,\mu_j] \ / \ (M-1) \qquad (C2)$$

where all charges were included in the sum over k because no significant difference was observed among the C_{ij} computed for individual charge bins. The charge resolution δZ was approximately 0.056 + 0.026 Z, plus a small rigidity-dependent correction term which applied for elements below neon. This resolution was obtained empirically to provide a flat S1-S2-S3-S4 confidence-level distribution from 0.05 to 1.00 (the distribution had a peak below 0.05 due to interactions and other backgrounds). The resolution agrees with that expected from photoelectron statistics, Symon-Landau energy-deposition fluctuations, and residual spatial non-uniformities in the scintillators. Although delta-ray channeling along magnetic field lines made the resolution slightly worse for S2, δZ applied satisfactorily to every scintillator. Confidence levels, for N-1 degrees of freedom, were calculated as the integral probability for expecting a chi square larger than χ_k^2 based on Gaussian statistics.

Seventy-two percent of the events had confidence levels for N = 4 which were above 0.05. These events were immediately accepted as non-interacting; the remainder were tested for agreement among S1 and any other two counters (i.e. N = 3). An event was accepted when treating 3 counters if the highest confidence level for such combinations was above 0.05. Scatter plots showed that most of the events in the S1-S2-S3 combination had interacted in S4, usually producing a lower pulse height there. Events with S1-S2-S4 or S1-S3-S4 agreement had the missing pulse large due to Landau energy fluctuations. Events failing the 3-counter agreement were checked in the same way for agreement between counters S1-S2, S1-S3, or S1-S4 (N = 2). The majority having 2-counter agreement were of the S1-S2 type, having interactions between S2 and S3.

REFERENCES

Abell, G. 1969, Exploration of the Universe (2nd ed.; N.Y.: Holt, Rhinehart, and Winston), p. 512.

Allen, C.W. 1955, Astrophysical Quantities (London: Athlone Press), p. 34.

Anand, K.C., Rengarajan, T.N., and Stephens, S.A. 1973, 13th Int. C.R. Conf., Denver, 1, 184.

Arens, J.F., and Ormes, J.F. 1975, Phys. Rev. D, 12, 1920.

Badhwar, G.D., and Osborn, R.W. 1974, Astrophys. and Spc. Sci., 28, 101.

Balasubrahmanyan, V.K., and Ormes, J.F. 1973, Ap. J., 186, 109.

Benegas, J.C., Israel, M.H., Klarmann, J., and Maehl, R.C. 1975, 14th Int. C.R. Conf., Munich, 1, 251.

Buffington, A., Orth, C.D., and Mast, T.S. 1978, submitted to Ap. J.

Buffington, A., Orth, C.D., and Smoot, G.F. 1974, Nucl. Instr. Meth., 122, 575.

________ 1975, Ap. J., 199, 669.

Caldwell, J.H. 1977, Ap. J., 218, 269.

Cameron, A.G.W. 1973, Space Sci. Rev., 15, 121.

Cassé, M., and Goret, P. 1973, 13th Int. C.R. Conf., Denver, 1, 584.

Cassé, M., Goret, P., and Cesarsky, C.J. 1975, 14th Int. C.R. Conf., Munich, 2, 646.

Cassé, M., Koch, L., Lund, N., Meyer, J.P., Peters, B., Soutoul, A., and Tandon, S.N. 1971, 12th Int. Conf. C.R., Hobart, 1, 241.

Chevalier, R.A. 1977, 15th Int. C.R. Conf., Plovdiv, invited lecture "C.R. Accel. in Supernova Remnants" and private communication.

Chevalier, R.A., Robertson, J.W., and Scott, J.S. 1976, Ap. J., 207, 450.

Cowsik, R., and Wilson, L.W. 1973, 13th Int. C.R. Conf., Denver, 1, 500.

Eberhard, P.H., and Koellner, W.O. 1972, Computer Physics Comm., 3, 296.

______ 1973, Loc. cit. 5, 163.

Golden, R.L., Adams, J.H., Badhwar, G.D., Deney, C.L., Lindstrom, P.J., and Heckman, H.H. 1974, Nature, 249, 814.

Júliusson, E. 1974, Ap. J., 191, 331.

Júliusson, E., Cesarsky, C.J., Meneguzzi, M., and Cassé, M. 1975, 14th Int. C.R. Conf., Munich, 2, 653.

Julliot, C., Koch, L., and Petrou, N. 1975, 14th Int. C.R. Conf., Munich, 12, 4118.

Lezniak, J.A., and Webber, W.R. 1975, 14th Int. C.R. Conf., Munich, 12, 4107.

Lezniak, J.A., Webber, W.R., Kish, J.C., and Simpson, G.A. 1977, 15th Int. C.R. Conf., Plovdiv, 1, 237.

Lindstrom, P.J. 1977, private communication.

Lindstrom, P.J., Greiner, D.E., Heckman, H.H., Cork, B., and Bieser, F.S. 1975a, Lawrence Berkeley Laboratory preprint #LBL-3650.

______________ 1975b, 14th Int. C. R. Conf., Munich, 7, 2315.

Lingenfelter, R.E., Ramaty, R., and Fisk, L.A. 1971, Astrophys. Lett., 8, 93.

Lund, N., Rasmussen, I.L., Peters, B., and Westergaard, N.J. 1975a, 14th Int. C.R. Conf., Munich, 1, 257.

Lund, N., Rasmussen, I.L., Peters, B., Rotenberg, M., and Westergaard, N.J. 1975b, 14th Int. C.R. Conf., Munich, 1, 263.

Maehl, R.C., Ormes, J.F., Fisher, A.J., and Hagen, F.A. 1977, Astrophys. and Spc. Sci., 47, 163.

Meneguzzi, M. 1973, 13th Int. C.R. Conf., Denver, 1, 378.

Meyer, P., Ramaty, R., and Webber, W.R. 1974, Physics Today, 27, No. 10, p. 23.

Ormes, J.F., and Balasubrahmanyan, V.K. 1973, Nature Phys. Sci., 241, 95.

Ormes, J.F., Fisher, A., Hagen, F., Maehl, R., and Arens, J.F. 1975, 14th Int. C.R. Conf., Munich, 1, 245.

Ormes, J., and Freier, P. 1978, Ap. J., to appear in 1 June issue.

Orth, C.D., and Buffington, A. 1976, Ap. J., 206, 312.

Orth, C.D., Buffington, A., and Smoot, G.F. 1975, 14th Int. C.R. Conf., Munich, 1, 280.

Orth, C.D., Buffington, A., Mast, T.S., and Smoot, G.F. 1977, Lawrence Berkeley Laboratory Report LBL-6422 (unpublished).

Owens, A.J. 1976a, Nature, 259, 344.

Owens, A.J. 1976b, Astrophys. and Spc. Sci., 44, 35.

Owens, A.J., and Jokipii, J.R. 1977, Ap. J., 215, 677 and 685.

Peters, B., and Westergaard, N.J. 1977, 15th Int. C.R. Conf., Plovdiv, 1, 435 (also see Danish Space Research Institute preprint BP/ba24/5-76).

Ramaty, R., Balasubrahmanyan, V.K., and Ormes, J.F. 1973, Science, 180, 731.

Rengarajan, T.N., Stephens, S.A., and Verma, R.P. 1973, 13th Int. C.R. Conf., Denver, 1, 384.

Saito, T., Sato, Y., Sugimoto, H., Matsubayashi, T., and Noma, M. 1974, J. Phys. Soc. Jap., 37, 1462.

Scott, J.S., and Chevalier, R.A. 1975, Ap. J. (Letts.), 197, L5.

Shapiro, M.M. and Silberberg, R. 1975, Phil. Trans. Roy. Soc. London, A277, 319.

Shapiro, M.M., Silberberg, R., and Tsao, C.H. 1975, 14th Int. C.R. Conf., Munich, 2, 532.

Silberberg, R., and Tsao, C.H. 1973, Ap. J. Supp., 25, #220, 315; and private communication.

Smith, L.H., Buffington, A., Orth, C.D., and Smoot, G.F. 1973a, 13th Int. C.R. Conf., Denver, 1, 177 (abstract).

Smith, L.H., Buffington, A., Smoot, G.F., Alvarez, L.W., and Wahlig, M.A. 1973b, Ap. J., 180, 987.

Smoot, G.F., Buffington, A., and Orth, C.D. 1975, Phys. Rev. Letts., 35, 258.

Smoot, G.F., Buffington, A., Orth, C.D., and Smith, L.H. 1973, 13th Int. C.R. Conf., Denver, 1, 225.

Von Rosenvinge, T.T., Webber, W.R., and Ormes, J.F. 1969, Astrophys. and Spc. Sci., 3, 4 and 80.

Weast, R.C., ed. 1972, Handbook of Chemistry and Physics (Cleveland: The Chemical Rubber Co.), 53rd ed., page E-56.

Webber, W.R., Damle, S.V., and Kish, J. 1972, Astrophys. and Spc. Sci., 15, 245.

Webber, W.R., Lezniak, J.A., and Kish, J. 1973a, 13th Int. C.R. Conf., Denver, 1, 248.

Webber, W.R., Lezniak, J.A., Kish, J.C., and Damle, S.V. 1973b, Nature Phys. Sci., 241, 96.

FIGURE CAPTIONS

1. Schematic drawing of the balloon-borne superconducting magnetic spectrometer.

2. Measured spectrum of average analog charges (uncorrected for interactions within the apparatus), including all events passing counter-agreement tests for 4, 3, and 2 counters. The sample includes all events with inverse rigidities from -0.02 to +0.30 $(GV/c)^{-1}$.

3. Energy dependences of the ratios (Z = 10+12+14)/(Z⩾25) and (15⩽ Z ⩽24)/(Z⩾25) at the top of the atmosphere, obtained from Table 4. The curves indicate the predictions based on the source abundances listed in Table 6 and the leaky-box model discussed in Section V with n = 0.5 and x_o = 4.3 g cm^{-2}.

4. Energy dependence of the O/C, (F+Na+Al)/(Ne+Mg+Si), and (Ne+Mg+Si)/(C+O) ratios at the top of the atmosphere, obtained from Table 4. The curves indicate the predictions based on the source abundances listed in Table 6 and the leaky-box model discussed in Section V with n = 0.5 and x_o = 4.3 g cm^{-2}.

5. Energy dependence of the ratio (Z⩾25)/(C+O) at the top of the atmosphere. The estimated uncertainty in our results due to systematic errors in the apparatus and atmospheric corrections is about 4% (cf. Table 3). The data of Anand et al. (1973) were not plotted because they cover only the range from 13 to 19 GV/c; the data of Golden et al. (1974) were omitted because their uncertainty is approximately 50%. The (23⩽Z⩽28)/(6⩽ Z⩽9) data of Ormes and Balasubrahmanyan (1973) have been multiplied by 0.96 to obtain an effective ratio for (Z⩾25)/(C+O), and were divided

by two in accordance with the revision of Arens and Ormes (1975). The (Z = 26+28)/(C+O) data of Webber et al. (1973a,b) have been multiplied by 1.1 to obtain a (Z⩾25)/(C+O) ratio. The data of Saito et al. (1974) were multiplied by 0.65 to convert to (Z⩾25)/(C+O). The data of Smith et al. (1973b, Table 7) were converted to energy per nucleon using their quoted bin edges, and the resulting (Z⩾25)/(C+O) ratio was multiplied by 1.3 for an atmospheric correction. The uncertainties shown for Saito et al. (1974) and Webber et al. (1973a,b) pertain to their published integral spectra, and are hence artificially small compared to those of the other experiments, which are differential. The curve is the prediction based on the source abundances listed in Table 6 and the leaky-box model discussed in Section V with n = 0.5 and $x_o = 4.3$ g cm^{-2}.

6. Energy dependence of the (Li+Be+B+N)/(C+O) ratio at the top of the atmosphere. Our results, from Table 4, have an overall normalization uncertainty of about 6% due to possible systematic error in the apparatus and atmospheric corrections (cf. Table 3). The data of Smith et al. (1973b, Table 7) were converted to energy per nucleon using their quoted bin edges, and the resulting (Li+Be+B+N)/ (C+O) ratio was multiplied by 0.77 for an atmospheric correction. The curve is the prediction based on the source abundances listed in Table 6 and the leaky-box model discussed in Section V with n = 0.5 and $x_o = 4.3$ g cm^{-2}.

7. Ratio of source abundances and solar-system abundances as a function of first ionization potential (cf. Table 6). The statistical errors shown ignore any contribution from uncertainties in the solar-system abundances.

A least chi-square fit (solid line) yields a source temperature of $(4.9 \pm 0.2) \times 10^4$ °K if we assume thermal equilibrium. This fit ignores the data point for Ne due to the large uncertainty in its solar abundance (Cassé et al. 1975). A much lower temperature is obtained for the dilute plasma model of Cassé and Goret (1973), as described in the text.

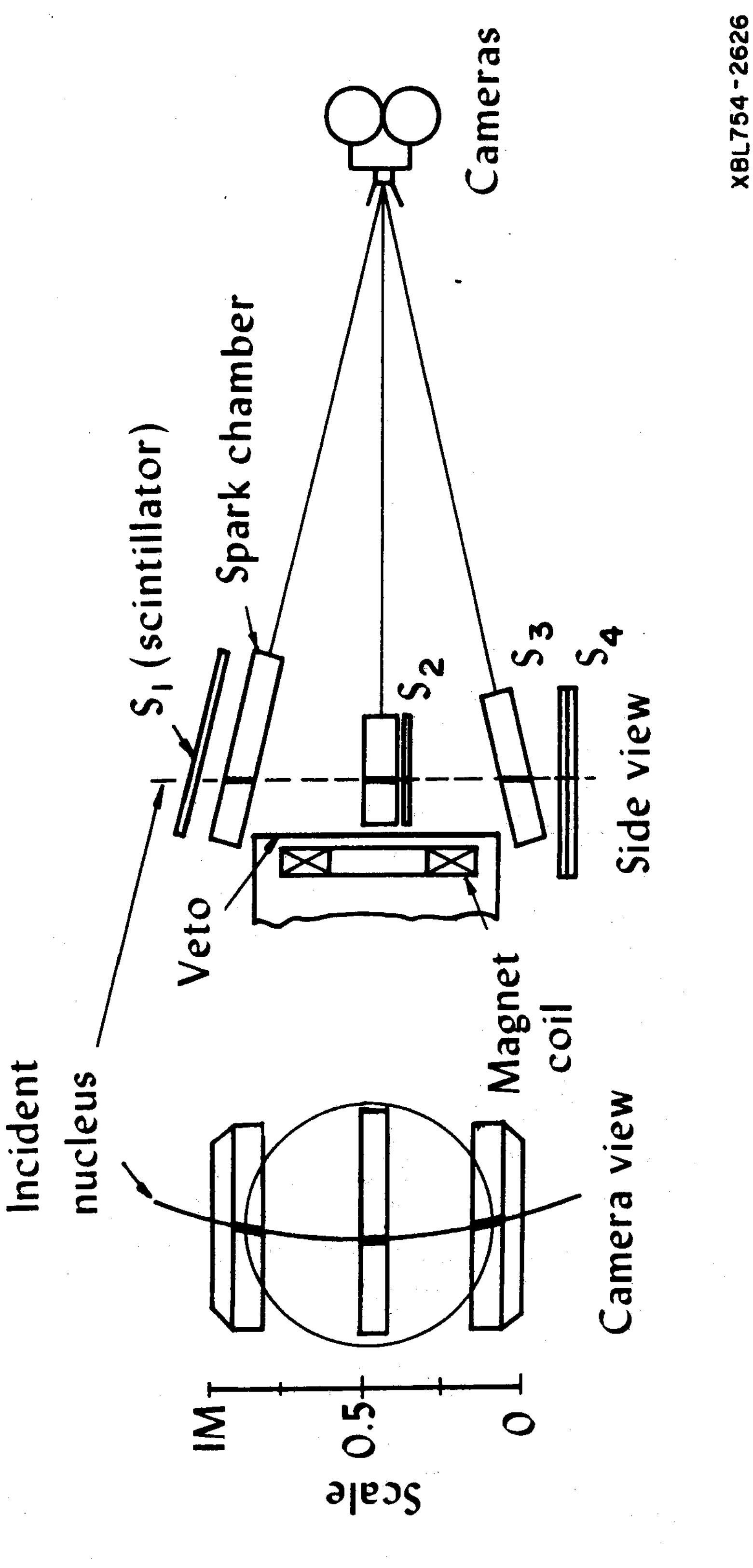
Cameras
Spark chamber
S_1 (scintillator)
S_2
S_3
S_4
Side view
Veto
Magnet coil
Incident nucleus
Camera view
Scale
IM
0.5
0
XBL754-2626

Figure 1.

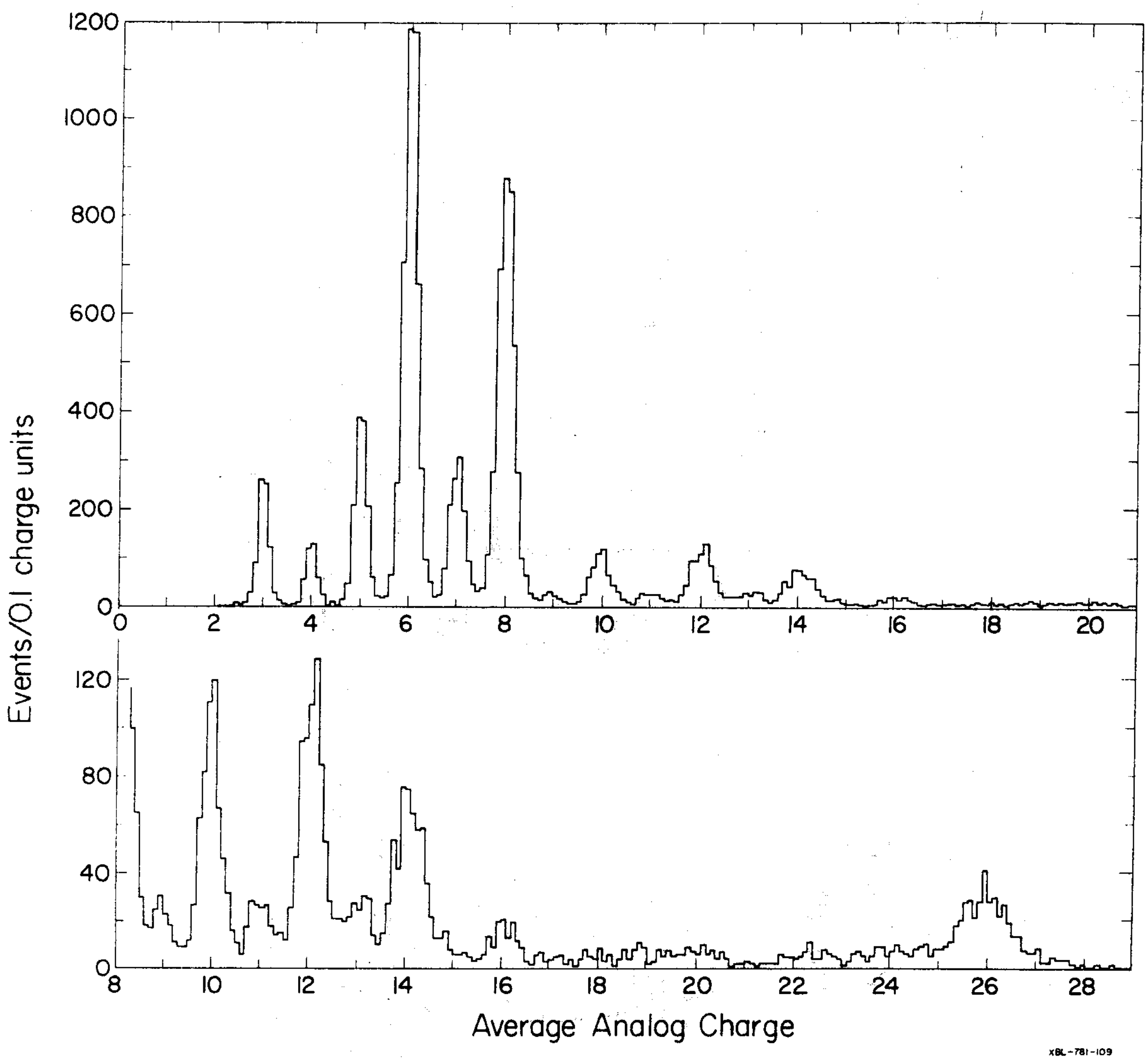

Events/0.1 charge units
1200
1000
800
600
400
200
0
0
2
4
6
8
10
12
14
16
18
20
120
80
40
0
8
10
12
14
16
18
20
22
24
26
28
Average Analog Charge
XBL-781-109

Figure 2.

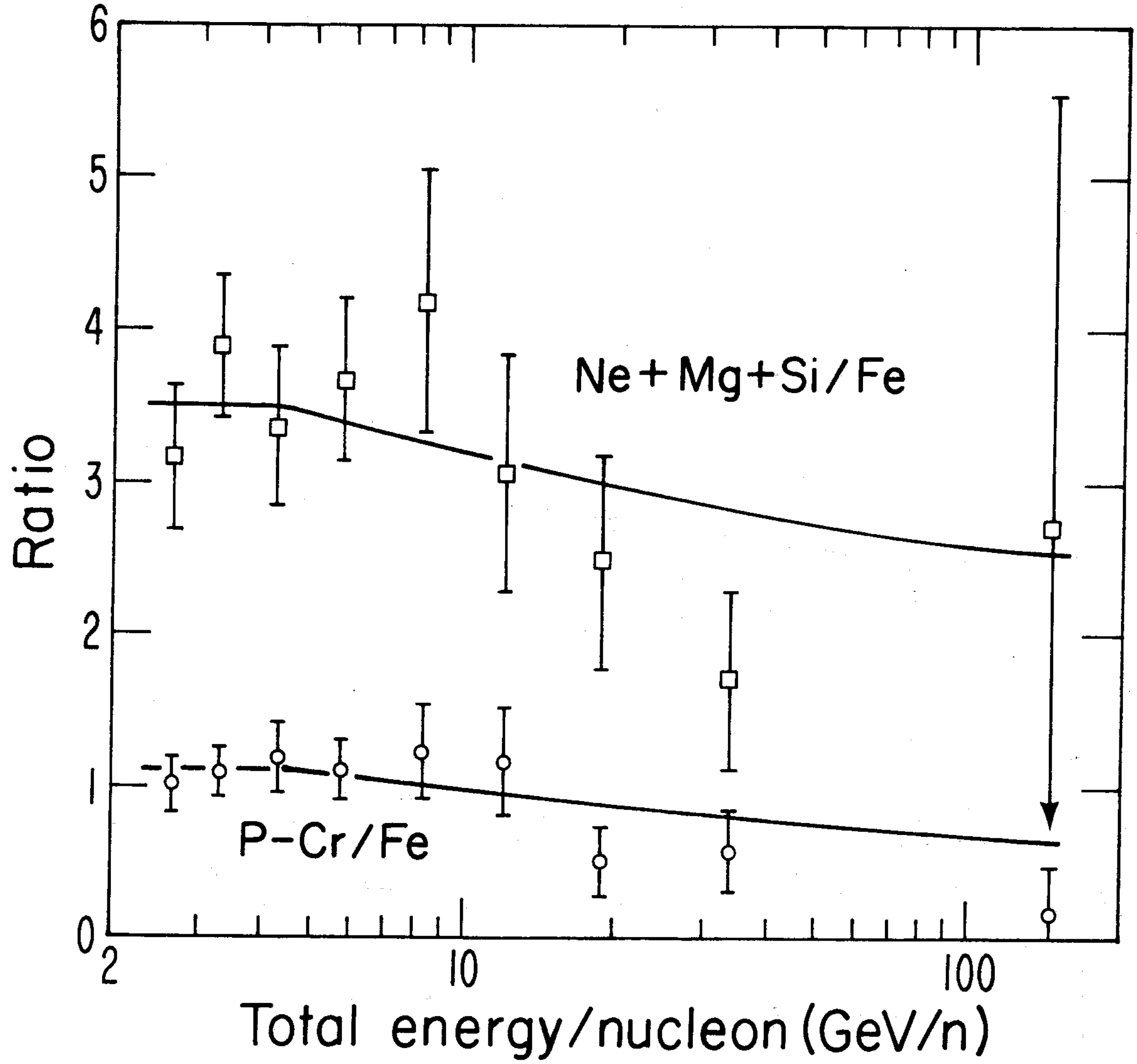
6
5
4
3
2
1
0
Ratio
Ne+Mg+Si/Fe
P-Cr/Fe
2
10
100
Total energy/nucleon (GeV/n)
XBL 783-2414

Figure 3.

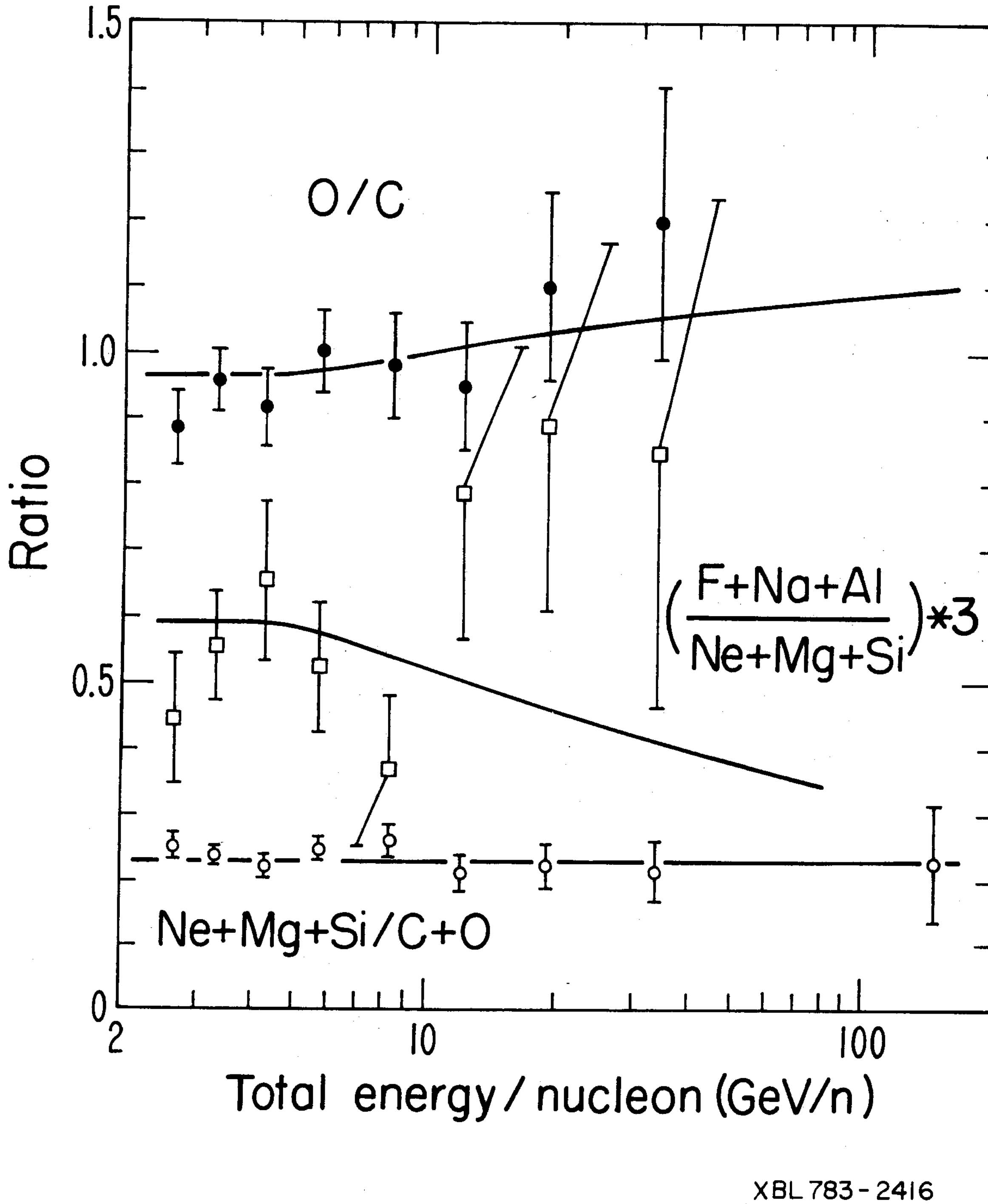
1.5
1.0
0.5
0
Ratio
O/C
(F+Na+Al / Ne+Mg+Si)*3
Ne+Mg+Si/C+O
2
10
100
Total energy / nucleon (GeV/n)
XBL 783-2416

Figure 4.

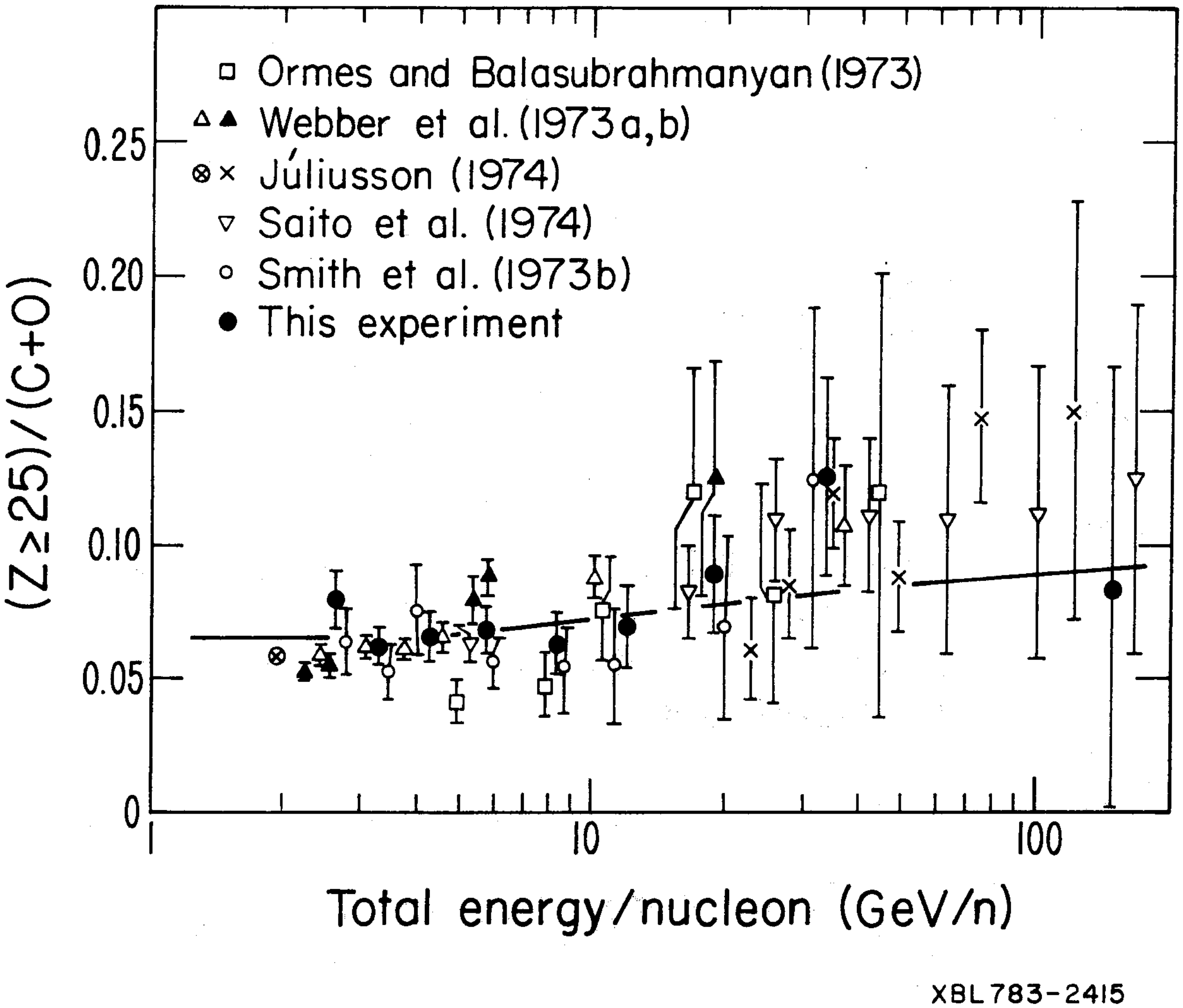

Ormes and Balasubrahmanyan (1973)
Webber et al. (1973a,b)
Júliusson (1974)
Saito et al. (1974)
Smith et al. (1973b)
This experiment
0.25
0.20
0.15
0.10
0.05
0
(Z≥25)/(C+O)
1
10
100
Total energy/nucleon (GeV/n)
XBL 783-2415

Figure 5.

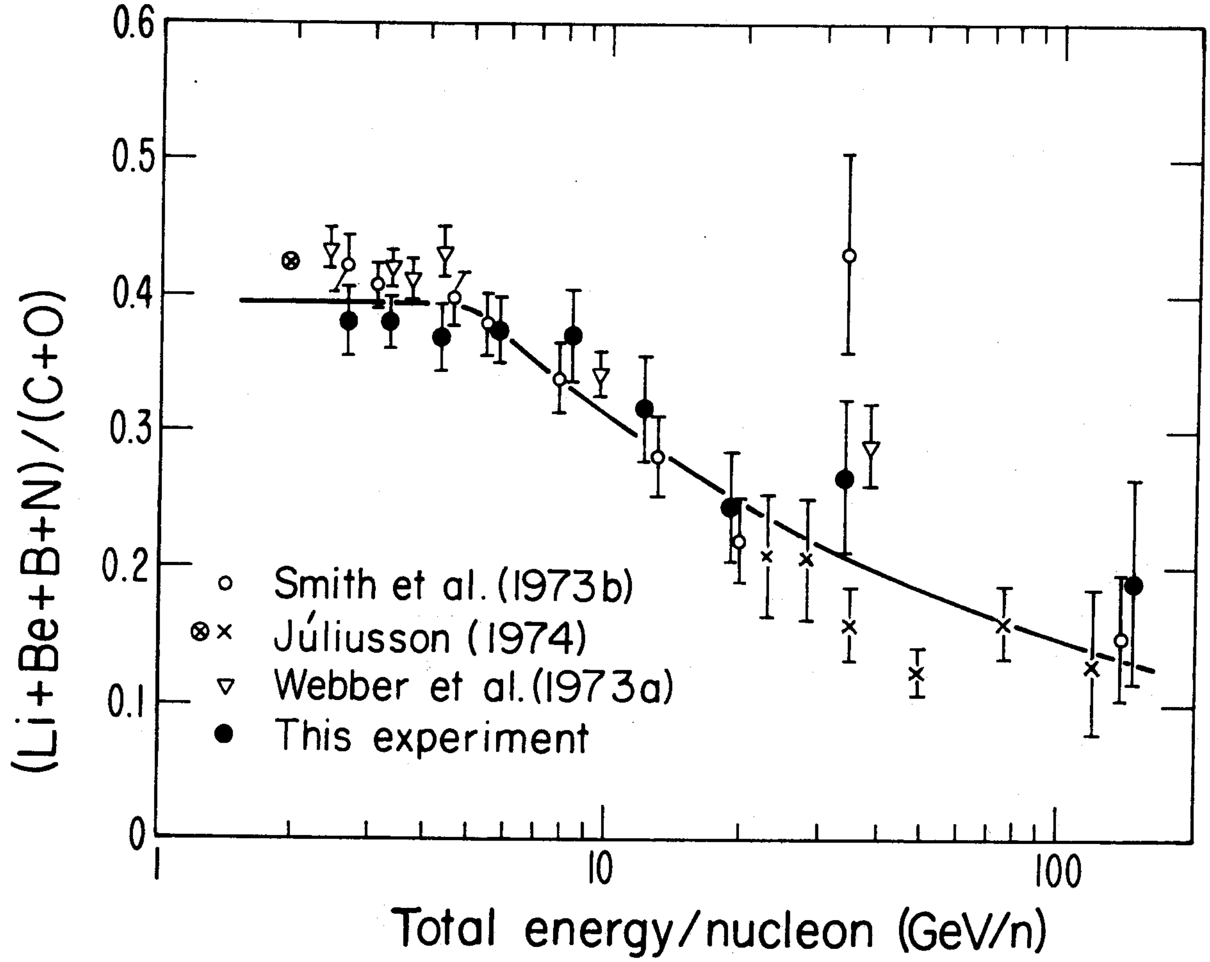

XBL 783-2413

Figure 6.

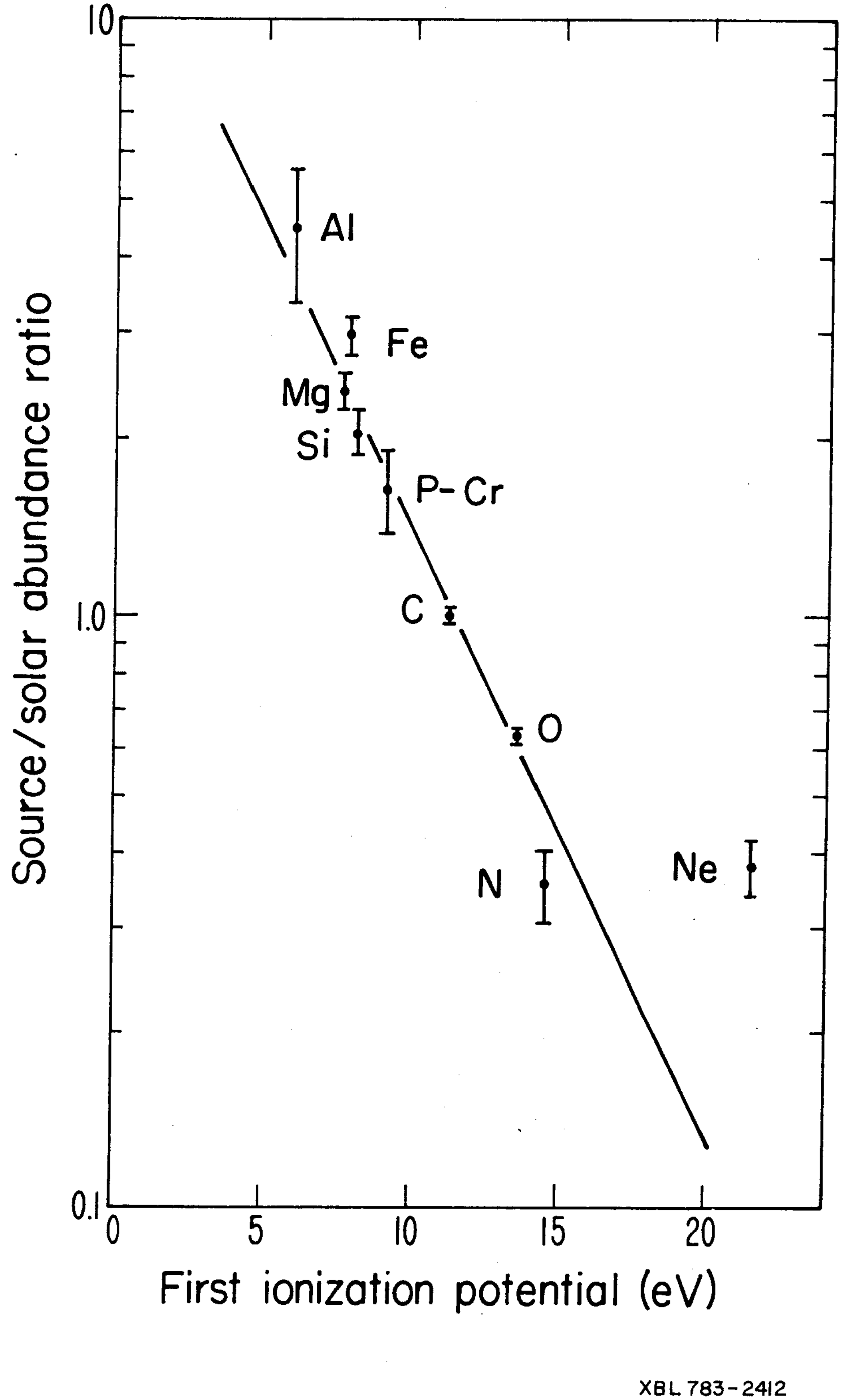
10
1.0
0.1
0
5
10
15
20
Source/solar abundance ratio
First ionization potential (eV)
Al
Fe
Mg
Si
P- Cr
C
O
N
Ne
XBL 783-2412

Figure 7.